引用格式：WU Zhiliang, CAI Nian, OU Weicheng, et al. High-precision Measurement for a Quantum Dot Encoder Based on Triangular-wave Skeleton Extraction of Coding Patterns[J]. Acta Photonica Sinica, 2023, 52(6):0612001
吴志良,蔡念,欧伟程,等.基于码道三角波骨架提取的量子点光栅尺高精度测量方法[J].光子学报,2023,52(6):0612001

基于码道三角波骨架提取的量子点光栅尺高精度测量方法

吴志良[1],蔡念[1],欧伟程[2],陈晓娜[1],王晗[2]
(1 广东工业大学 信息工程学院,广州 510006)
(2 广东工业大学 机电工程学院,广州 510006)

摘　要:为了提高量子点光栅尺的测量精度,提出了一种基于码道三角波骨架提取的位移测量方法。根据量子点光栅尺码道图案具有蜿蜒、连续的形状特点,利用不定长边缘跟踪方法快速检测出码道边缘。对码道中线进行三角波拟合得到码道骨架,提升测量稳定性以及位移值细分线性度。利用径向基神经网络对非线性测量误差进行补偿。所提出的测量方法比已有测量方法具有更好的测量精度和效率。

关键词:机器视觉;量子点光栅尺;测量;边缘跟踪;骨架提取
中图分类号:TP391　　**文献标识码**:A　　**doi**:10.3788/gzxb20235206.0612001

0 引言

高端微纳制造与测量是先进制造领域的重要研究方向,受到国际学术界和工控产业界的高度重视[1]。如何实现高精度位移测量是高端制造装备制造的关键环节[2-6]。目前,激光干涉仪和光栅尺常被用于高精度位移测量[7-10]。前者可通过计数和细分干涉条纹实现亚微米级测量,但对测量环境要求苛刻[11-12],且光学零件繁多难以直接集成于装备内部,极大地限制了其在工业测控领域的应用。相对于激光干涉仪,光栅尺[13]具有低成本、小体积、高精度的优点,被作为核心位移测量器件而广泛集成于精密制造装备。当今,大批量稳定制造光栅的方法主要有机械刻栅、光刻刻栅等[14-20]。可是,这些成熟工艺具有成品率低,生产周期长、生产条件严苛等缺点。而且,采用这些工艺制造出来的光栅尺在长时间运作后,光源模块会产生大量热导致光栅尺内部温度变化剧烈,引起光栅基底(即码道)的热形变误差,影响其测量精度[30]。为了规避现有光栅尺的制栅工艺缺陷,本研究团队采用微纳增材制造开发出一款新型量子点光栅尺[31],其工作原理是将增材制造喷印在基底上的自发光量子点码道图案作为信息载体,运用机器视觉方法对该连续、规则、蜿蜒的量子点码道图案进行实时处理而实现位移测量。

类似于现有光栅尺测量,量子点光栅尺在测量过程中也不可避免地会受到测量硬件偶然误差(如尺身污染、光电不稳定性、工装误差)、外界温度、振动等因素的干扰[23-26],从而影响测量精度。已有不少研究探索测量方法和误差抑制方法,以提升现有光栅尺的重复定位与绝对定位精度[27-30]。李彦锋等[27]利用基于虚拟仪器的宏微复合光栅尺测量系统代替莫尔条纹的电子细分方法。CAI N等[28]利用经验模态分解方法分解出本征模函数来描述轮廓变化的趋势,进而得到一个自适应阈值以划分光栅精细边缘。LI W等[29]基于经验模态分解和局部正弦辅助方案提出一种光栅尺非线性误差补偿方法,提升了绝对式光栅尺测量精度。BARAKAUSKAS A等[30]建立一种新的数值模型解决光栅尺在非理想环境下的振动误差。但是,量子点光

基金项目:国家自然科学基金(No. 62171142),广东省自然科学基金(No. 2021A1515011908),惠州市高校科研专项资金项目(No. 2019HZKY003)
第一作者:吴志良,2112003056@mail2.gdut.edu.cn
通讯作者:蔡念,cainian@gdut.edu.cn
收稿日期:2022-12-22;**录用日期**:2023-02-20

栅尺的量子点码道图案与现有光栅尺的黑白相间光栅条纹在外观上具有极大的差异性，前者表现为连续且规则的蜿蜒形状，因此难以将现有光栅尺的测量方法直接应用于量子点光栅尺。

为进一步提高量子点光栅尺的测量精度，本文提出一种基于码道三角波骨架提取的量子点位移测量方法。采用不定步长边缘跟踪方法快速、有效地检测出量子点光栅尺码道边缘。为了确保算法稳定性和较好的细分线性度，采用三角波拟合方法提取量子点光栅尺码道骨架。采用一种由粗到精的位移检测方法，准确地进行位移测量。最后，采用径向基神经网络进行非线性测量误差补偿，减少绝对位移误差。

1 量子点光栅尺简述

图1为量子点光栅尺的内部结构及其测量工作原理。图2为量子点光栅尺光信号采集系统，采集的码道呈现连续、规则的蜿蜒形状，在365 nm波长的紫外光线照射下实现光致发光。在文献[31]中，采用机器视觉方法对码道图案进行处理实现高精度测量，即简单地对粗位移值与精位移值两个数据量进行同步解耦：采用蜿蜒波峰个数累加法获得粗位移值，采用像素点细分方法获得细位移值。虽然这种位移测量方法已经达到设计要求[31]，但是仍然距离高精度需求较长距离。因此，本文提出一种新的高精度位移测量方法，进一步提升量子点光栅尺的测量精度。

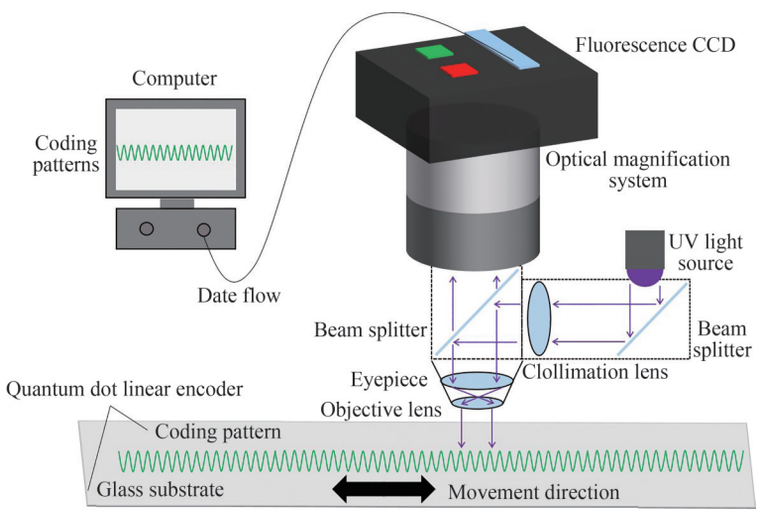

图1 量子点光栅尺的位移测量原理[31]

Fig.1 Displacement measurement principle of quantum dot encoder[31]

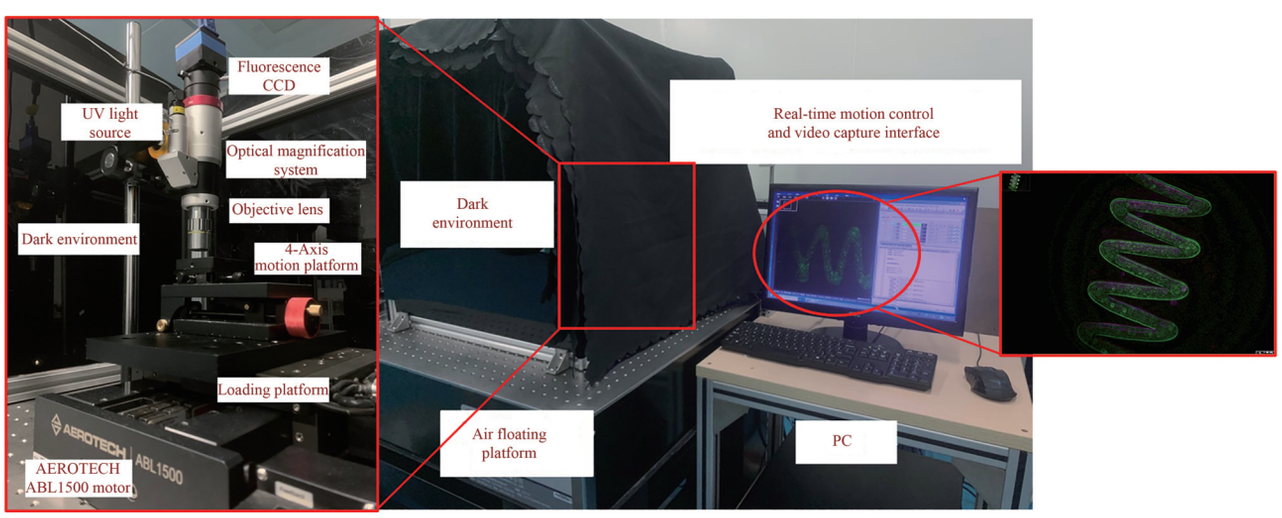

图2 量子点光栅尺光信号采集系统

Fig.2 Signal capture system for the quantum dot encoder

2 方法与理论

本文提出的量子点光栅尺位移测量方法主要包括码道图像预处理、码道检测、码道骨架提取和位移测量等四个步骤，如图3所示。首先对采集到的码道图像进行自适应二值化预处理；然后提出不定步长边缘跟踪方法检测码道轮廓；之后，由码道轮廓获得码道中线，采用三角波对码道中线进行拟合得到码道骨架；最后，在位移测量步骤，先采用宏微复合测量方法分别测量码道粗位移值和精细位移值，再采用径向基神经网络进行非线性误差补偿，最终获得精确位移值。

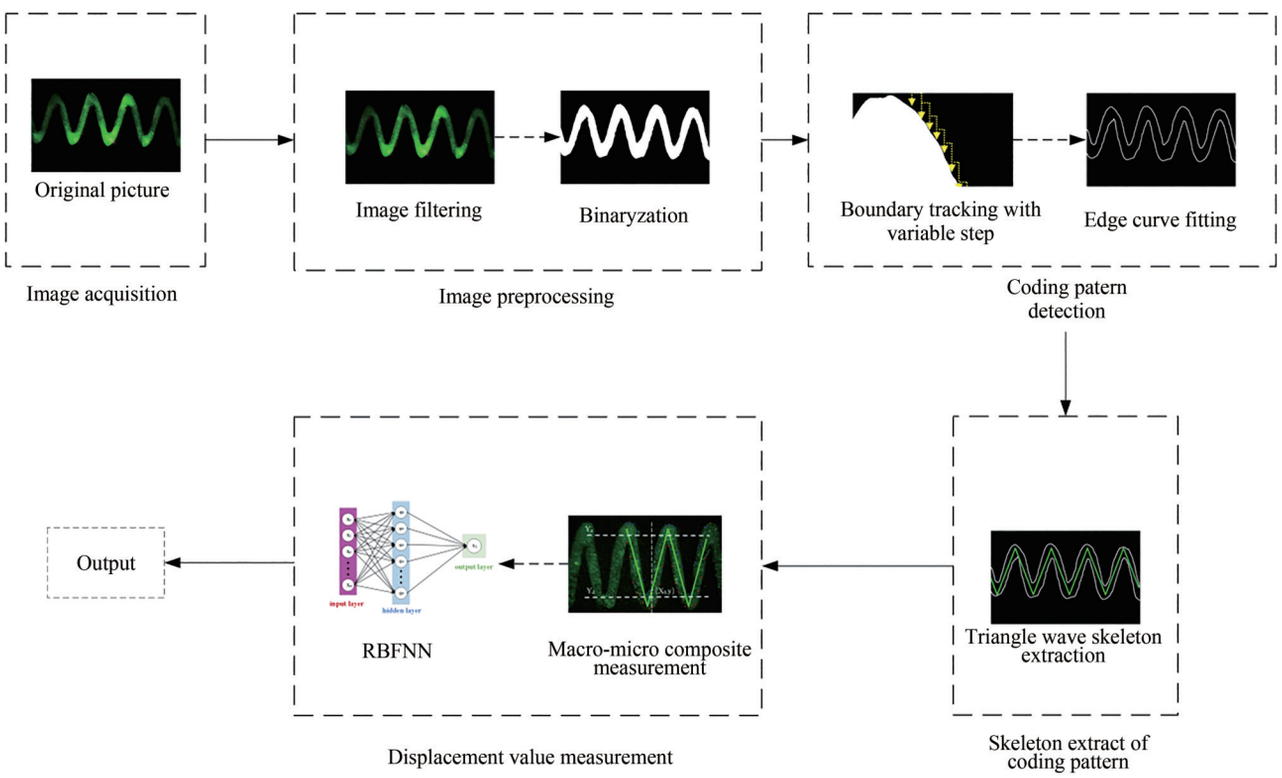

图3 位移测量方法流程图

Fig.3 Pipeline of the proposed measurement method

2.1 基于不定步长边缘跟踪的码道检测

考虑到量子点光栅尺码道呈现蜿蜒状且连续的形状特性，提出不定步长边缘跟踪方法检测码道上下边缘（如图4所示）。相比于传统边缘跟踪算法，不定步长边缘跟踪方法在边缘跟踪方向判断时只需判断右上和右下两个方向，大大加快了边缘跟踪速度。为了进一步提升算法效率，先检测出离散边缘点再拟合出完整码道边缘。需要注意的是，相比于码道的其他位置，在码道波峰及波谷处需设计较小的检测步长，以实现码道波峰波谷的精确检测。以上边缘跟踪为例，对不定步长边缘跟踪方法进行概述。

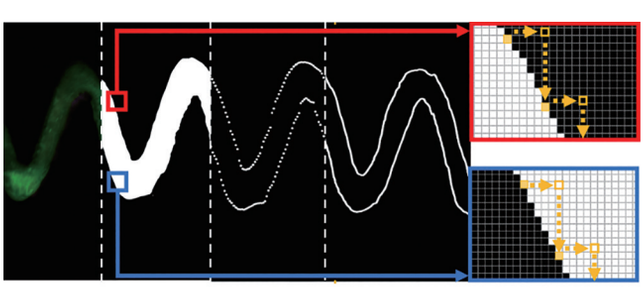

图4 码道轮廓检测

Fig.4 Contour detection of the coding pattern

1)确定起始点。对一张二值化码道图像,从待检测区域的最左上角像素开始,往下扫描找到第一个像素值为255的点为起始点,记为$P_0(x_0,y_0)$。

2)确定下一个边界点。记$P_1(x_1,y_1)=(x_0+1,y_0+1)$。若$P_1=0$,则码道边缘位于$P_1$右下方,此时先由$P_1$向右搜索至$P_2(x_1+n,y_1)$,再一直往下搜索至检测区域下边界,找到第一个像素值为255的点,记为P_3;若$P_1=255$,则码道边缘位于P_1右上方,此时P_1向右搜索至P_2后再一直往上搜索至检测区域上边界,找到最后一个像素值为255的点,记为P_3。

3)逐点跟踪。将P_3标记为P_0,重复步骤2),直至搜索点到达检测区域的右边界或下边界则跟踪停止,获得码道边缘离散点$[x_i,y_i](i=0,1,2,\cdots,n)$。

4)码道边缘连接。首先计算步长h_i

$$h_i=x_{i+1}-x_i\quad(i=0,1,2\cdots,n) \tag{1}$$

然后将边缘离散点以及步长h_i,代入

$$\begin{bmatrix}-h_1 & h_0+h_1 & -h_0 & \cdots & \cdots & 0\\ h_0 & 2(h_0+h_1) & h_1 & 0 & \cdots & \vdots\\ h_1 & h_1 & 2(h_0+h_1) & h_2 & 0 & \vdots\\ \vdots & 0 & \ddots & \ddots & \ddots & 0\\ 0 & \cdots & 0 & h_{n-2} & 2(h_{n-2}+h_{n-1}) & h_{n-1}\\ 0 & \cdots & \cdots & -h_{n-1} & h_{n-2}+h_{n-1} & h_{n-2}\end{bmatrix}\begin{bmatrix}m_0\\ m_1\\ m_2\\ m_3\\ \vdots\\ m_n\end{bmatrix}=6\begin{bmatrix}0\\ \dfrac{y_2-y_1}{h_1}-\dfrac{y_1-y_0}{h_0}\\ \dfrac{y_3-y_2}{h_2}-\dfrac{y_2-y_1}{h_1}\\ \vdots\\ \dfrac{y_n-y_{n-1}}{h_{n-1}}-\dfrac{y_{n-1}-y_{n-2}}{h_{n-2}}\\ 0\end{bmatrix} \tag{2}$$

将式(2)求解得到的m_i代入

$$a_i=y_i \tag{3}$$

$$b_i=\frac{y_{i+1}-y_i}{h_i}-\frac{h_i}{2}m_i-\frac{h_i}{6}(m_{i+1}-m_i) \tag{4}$$

$$c_i=\frac{m_i}{2} \tag{5}$$

$$d_i=\frac{m_{i+1}-m_i}{6h_i} \tag{6}$$

求解式(3)~(6)获得样条曲线系数a_i,b_i,c_i,d_i。则任意两个邻近离散边缘点x_i和x_{i+1},采用式(7)获得两者之间的插值$g_i(x)$即可获得连续边缘值

$$g_i(x)=a_i+b_i(x-x_i)+c_i(x-x_i)^2+d_i(x-x_i)^3 \tag{7}$$

2.2 基于三角波拟合的码道骨架提取

经过2.1节所述码道边缘检测方法后,分别得到码道上、下边缘像素坐标序列$y_{ul}(x)$和$y_{dl}(x)$。考虑到光栅尺的高速测量,提出一种简单高效的码道中线提取方法得到码道中线$y_{ml}(x)$,

$$y_{ml}(x)=\frac{1}{2}\times[y_{ul}(x)+y_{dl}(x)] \tag{8}$$

在量子点光栅尺制造时,采用四轴运动平台按照设计移动光栅尺基底,使得喷头打印或喷印在基底上的量子点呈现连续、规则、蜿蜒的码道图案。因为运动平台自身限制,其运动轨迹更趋向于三角波方式行进,所以对码道中线用最小二乘法进行三角波拟合后得到码道骨架,如图5所示。

具体实现如下:对码道中线共m个样本点数据(x_i,y_i)进行三角波拟合,即

$$f(x_i;a,b,c,T)=\begin{cases}-4/T\times(x_i-b\%T))+1+c/a & ((x_i-b)\%T<T/2)\\ 4/T\times(x_i-b\%T))-3+c/a & ((x_i-b)\%T>T/2)\end{cases} \tag{9}$$

如式(9)拟合的数据满足

$$\min\sum_{i=1}^{m}\left[\boldsymbol{y}_i-\boldsymbol{f}(\boldsymbol{x}_i;\boldsymbol{a},\boldsymbol{b},\boldsymbol{c},\boldsymbol{T})\right]^2 \tag{10}$$

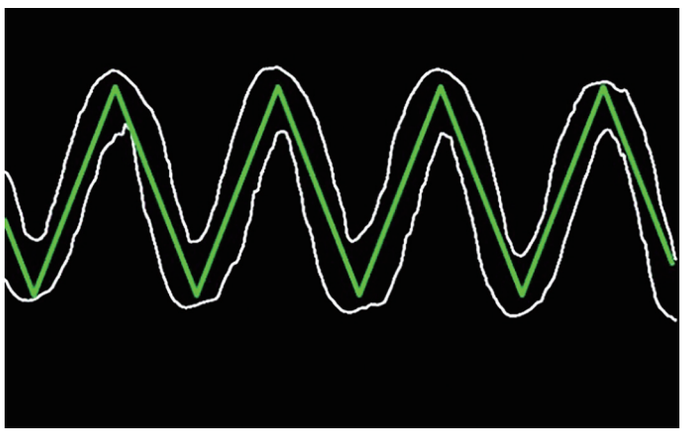

图5　码道骨架提取
Fig.5　Skeleton extraction of the coding pattern

则三角波拟合得到码道骨架。

虽然这种三角波拟合的码道骨架提取方法能够满足光栅尺测量的时效性，但是会产生一定的测量误差，因此在后面将引入快速非线性误差补偿来提升测量精度。

2.3　位移测量

对码道骨架采用由粗到精的码道位移计算方法计算位移值N_{xs}

$$N_{xs}=N_{x1}+N_{x2} \tag{11}$$

式中，N_{x1}、N_{x2}分别为码道粗位移值和细位移值，将在下面进行阐述。

2.3.1　码道粗位移值

待量子点光栅尺归零后，将图像最清晰区域作为感兴趣区域（Region of Interest，ROI），将ROI内最左边的码道骨架波峰对应的x轴坐标x_0所在列作为固定观测位，如图6白色竖直虚线所示。当量子点光栅尺发生位移时，码道骨架的波形相位也会相应发生变化，此时x_0位置对应的y值也会发生变化（如图6右图所示）。为提高解码的抗干扰能力，降低误码率和丢码率，设立上下两个阈值Y_u和Y_d。当且仅当观测位(x_0,y)的y值先小于Y_d，再大于Y_u，认为码道位移经过了一个码元。

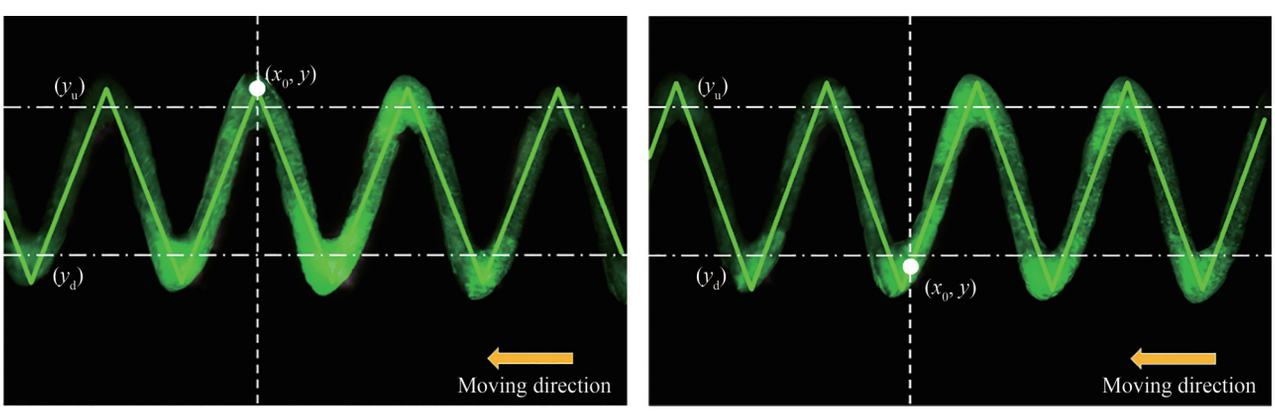

图6　位移测量
Fig.6　Displacement measurement

每半个码元经过一次观测位，计数器$\bar{T}$累加一次，作为粗测量值N_{x1}，即

$$N_{x1}=\frac{\bar{T}}{2}\times L_p \tag{12}$$

式中，L_p为码元长度。

2.3.2 码道精细位移值

精细位移值N_{x2}根据观测点距离最近波峰的长度来决定，即

$$N_{x2}=\left(x_0-x_{N_{x1}}\right)\times L_{\mathrm{pix}} \tag{13}$$

式中，$x_{N_{x1}}$为距离观测位(x_0,y)最近波峰的x轴坐标，L_{pix}为每个像元的物理长度。

2.3.3 位移非线性补偿

对同一码道进行多次测量，得到n组测量数据N_{xs}^n，即可获得测量平均数据$\overline{N_{xs}^n}$。

$$\overline{N_{xs}^n}=\frac{1}{n}\times\sum_{n=1}^{n}N_{xs}^n \tag{14}$$

因为测量环境影响，测量平均数据$\overline{N_{xs}^n}$与真实位移值x_T具有一定偏差。因为径向基神经网络具有结构简单、收敛速度快、容易部署、对非线性函数具有良好逼近性能等优点，所以采用径向基神经网络（如图7所示）进行非线性补偿，即将$(\overline{N_{xs}^n},x_T)$作为网络的训练样本和真实值输入，即

$$\varphi(x)=k\left(\left|\left|\overline{N_{xs}^n}-x_{\mathrm{c}}\right|\right|\right)=\mathrm{e}^{\frac{-\|N_{xs}-x_{\mathrm{c}}\|^2}{2\sigma^2}} \tag{15}$$

式中，x_{c}和σ分别为径向基函数$\varphi(x)$的核和方差，经过网络训练确定其参数值。后续测量将位移值N_{xs}直接输入到训练好的径向基神经网络，进行非线性误差补偿获得量子点光栅尺的精确位移值。

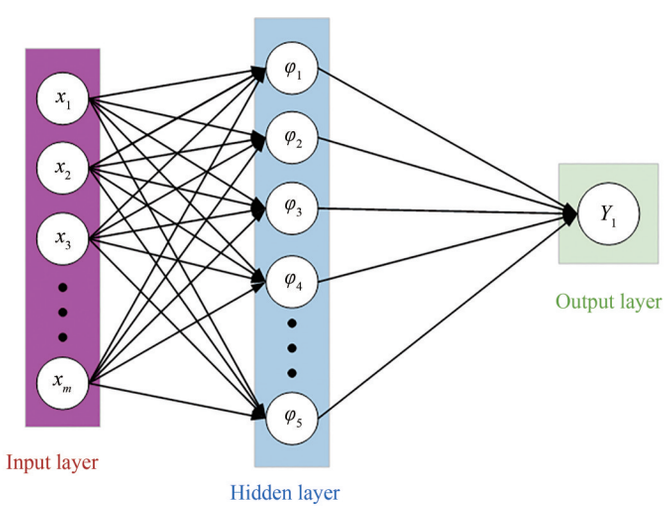

图7 径向基神经网络

Fig. 7 Radial basis function neural network

3 实验

3.1 实验平台

量子点光栅尺选用荧光CCD组件（广州明美，Mshot MS23）作为光信号读数头，在完成荧光CCD与码道的对焦后即实现量子点自发光图像采集。随后，将高精度直线电机（美国AREOTECH，ABL1500）作为光栅尺的运动载体进行定向运动，直线电机通过螺栓固定于大理石气浮平台上，避免外界与人为制造的过大抖动引入外界干扰误差。使用激光干涉仪（型号为Keysight 5519系列，定位精度±0.1 μm）作为参照标准。实验在黑暗遮光罩内执行，实验温度为20 ℃。量子点光栅尺测量系统如图8所示，位移测量方法执行硬件和软件环境配置如表1所示。

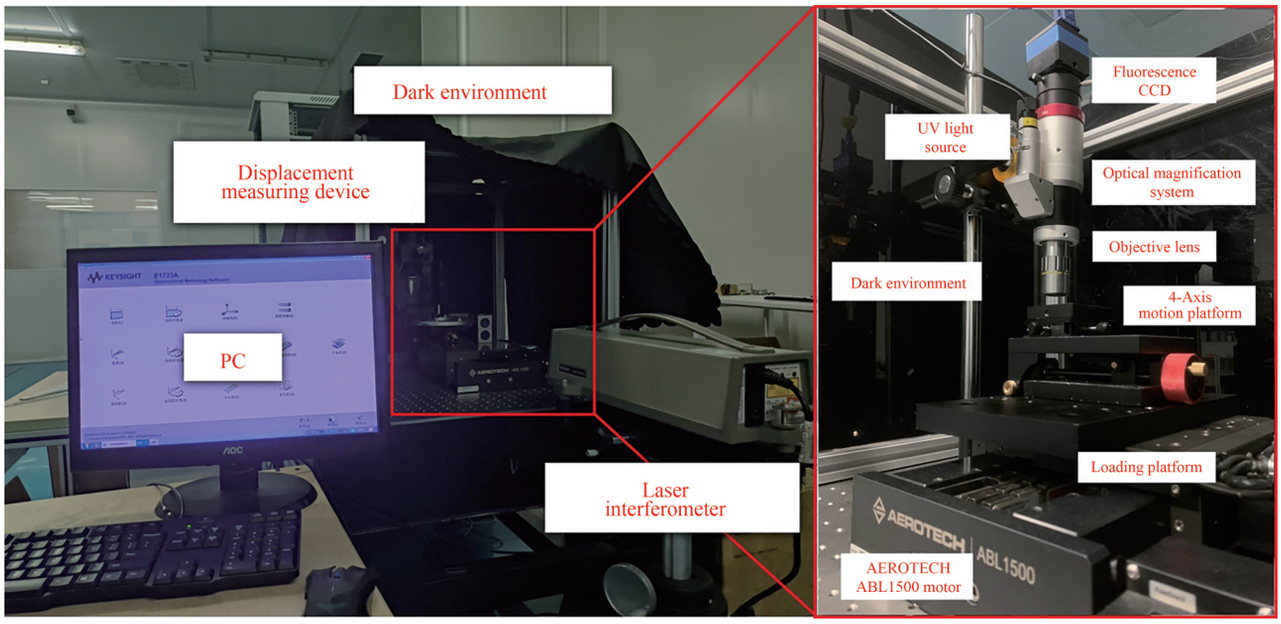

图8　量子点光栅尺测量系统

Fig.8　Measurement system of the quantum dot encoder

表1　位移测量方法执行硬件和软件环境配置

Table 1　Hardware and software environment configurations of the displacement measurement method

Equipment and software	Parameters
CPU	AMD Ryzen 7 5800 8-Core 3.40 GHz
GPU	NVIDIA GeForce RTX 3060 12 GB
Operating system	Windows 10
OpenCV	4.0.1
Python	3.6

3.2　评价指标

为了客观地验证本文方法，使用均方根误差（Root Mean Square Error，RMSE）、误差绝对值的最大值（Max Error）及方差（Variance）、重复定位误差（Rep Error）、95% 置信区间（Confidence Interval，CI）、运行时间（Running time）这六个指标进行评价。重复定位误差表示量子点光栅尺在同一位移距离下测量值之间的偏移值。均方根误差计算公式为

$$\mathrm{RMSE}=\sqrt{\frac{1}{N}\sum_{i=1}^{N}\left(h(x_i)-y_i\right)^2} \tag{16}$$

式中，$h(x_i)$表示位移测量算法输出的测量值，y_i表示用激光干涉仪测量出的基准值。

置信区间计算公式为

$$\begin{cases}\mathrm{lower}=\mathrm{Mean}-z\cdot\mathrm{ST}\\ \mathrm{upper}=\mathrm{Mean}+z\cdot\mathrm{ST}\end{cases} \tag{17}$$

式中，lower表示置信区间下限，upper表示置信区间上限，Mean为平均定位误差，ST为测量误差的标准差。当取95% 置信区间时，z值为1.96。

3.3　波形拟合讨论

为了验证三角波拟合的有效性，采用最小二乘法分别将码道中线拟合成三角波、正弦波和方波，拟合效果如图9所示，对测量影响如表2所示，其中RMSE表示拟合波形与码道中线的均方根误差。从表2可知，三角波拟合后的测量信号幅度最大，其测量信号的均方根误差远小于方波拟合而稍大于正弦波拟合。RMSE过大表明拟合后的波形发生了严重失真，如图9(c)的方波拟合信号所示。

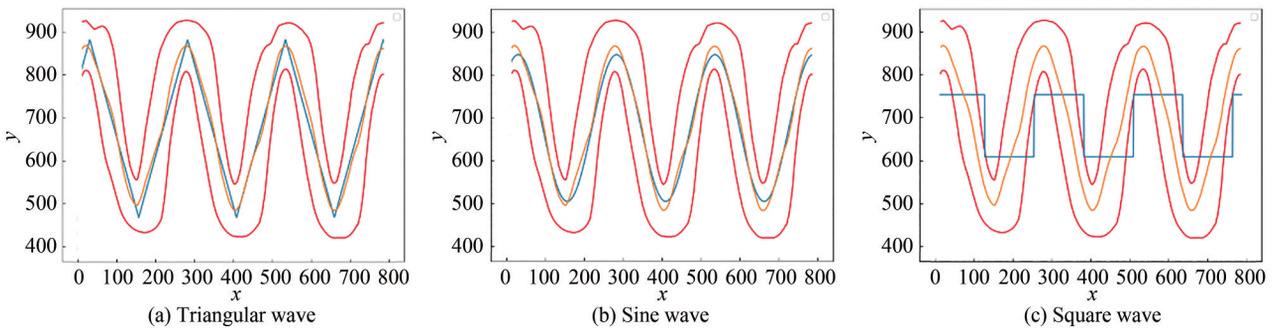

图9 波形拟合对比

Fig.9 Comparisons of different waveform fittings

表2 波形拟合结果对比

Table 2 Comparisons of fitting results via different waveforms

Waveform	RMSE/pixel	Amplitude/pixel
Square wave	106.24	73
Sine wave	37.99	171
Triangular wave	38.49	207

由于在实际测量中阿贝误差和余弦误差[21]的产生是难以避免的，将造成量子点光栅尺的码道发生相对位置偏移。当码道竖直方向偏移过大，造成拟合后的波峰低于图6所示的上阈值Y_u，或波谷高于Y_d时就会产生丢码。同时，上下阈值之间不宜设置得过于接近，以防止测量中因抖动而产生误码。因此更大的幅值可以使得上下阈值有更广的设置范围，从而降低误码率。因此，在三角波与正弦波的均方根误差相差不大的情况下，本文选择幅值更大的三角波拟合测量信号。

3.4 神经网络对误差补偿的作用

为了验证径向基神经网络对量子光栅尺测量误差补偿的作用，在其他实验条件不变的前提下，使用Back Propagation（BP）网络、长短期记忆网络（Long Short-Term Memory，LSTM）网络以及径向基神经网络分别对测量位移数据进行补偿处理。由表3可以看出，径向基神经网络在误差补偿性能上优于其余两个神经网络。

表3 不同神经网络用于量子点光栅尺误差补偿

Table 3 Comparisons of error compensation for the quantum dot encoder via different neural networks

Method	RMSE/μm	Max error/μm	Variance/μm^2	CI
BPNN	11.562	21.543	36.617	[−23.568,6.0183]
LSTM	21.920	48.190	133.512	[−15.499,46.129]
RBFNN	0.551	0.988	0.183	[−1.193,0.885]

3.5 消融实验

本节进行消融实验分析提出的位移测量方法中的三个不同步骤对位移测量的影响。以文献[31]的位移测量方法为基础方法，增加不同步骤以说明各自对位移测量的影响。为了方便描述，将基于不定步长边缘跟踪的码道检测简称为BTVS（Boundary Tracking with Variable Step，BTVS）；基于三角波拟合的码道骨架提取检测简称为（Triangular Wave Skeleton Extraction，TWSE）；径向基神经网络简称为RBFNN（Radial Basis Function Neural Network，RBFNN）。同时，我们重复了10组对比实验进行统计分析。

1）BTVS步骤讨论

BTVS的检测路径一直保持在码道边缘周围，因此只需要遍历很少的像素点即可检测出边缘。从表4可以看出，当融入BTVS时，基础方法的运行时间可以从42.13 ms缩减到20.17 ms，运行效率提升了108.86%。

2）TWSE步骤讨论

表4　消融实验

Table 4　Ablation experiments

Method	RMSE/μm	Max error/μm	Rep error/μm	Variance/μm²	CI	Running time/ms
Pre [31]	10.166	30.1745	±8.695	41.49	[−20.875, 18.813]	42.13
Pre+BTVS	18.142	54.800	±33.476	135.838	[−39.243, 16.989]	20.17
Pre+TWSE	6.352	19.741	±0.870	14.853	[−12.568, 2.410]	46.17
Pre+RBFNN	3.488	16.426	±13.395	6.336	[−7.008, 6.668]	43.35
Ours	0.551	0.988	±0.870	0.183	[−1.193, 0.885]	24.32

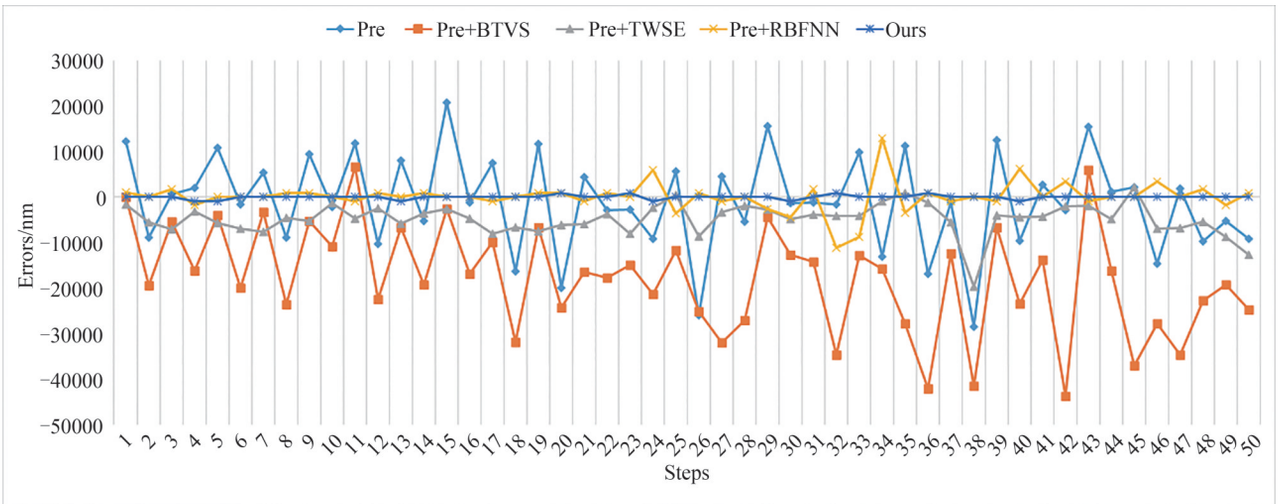

图10　各方法误差对比

Fig.10　Measurement errors obtained by five methods

当基础方法增加了TWSE之后，除了运行效率略有下降，其余指标均得到提升。这是因为使用三角波拟合得出码道骨架后，首先使得码元之间有了精细明确的分界点；其次，由于三角波为一次函数，使得测量结果有较好的细分线性度；最后，因为使用了最小二乘法拟合波形，因此只有当检测出的码道中线在噪声环境下整体或大部分数据发生偏移，才会使得拟合波形发生变化，这使得码道骨架具有较高稳定性，体现在位移测量方法的重复定位误差由±8.695 μm降低到±0.870 μm。

3）RBFNN步骤讨论

当基础方法融入了RBFNN之后，RMSE、Max Error、方差、CI等指标均得到提升，说明RBFNN可以有效地补偿量子点光栅尺非线性误差。

由表4看出，本文提出的位移测量方法大幅度地提升了测量速度，而且各项测量指标远优于文献[31]，这说明本文融合了BTVS、TWSE、RBFNN三个步骤后，综合提升了其测量性能。

4　结论

本文提出了一种基于码道三角波骨架提取的量子点光栅尺高精度测量方法。该方法利用不定步长边缘跟踪方法提升算法运行效率，提取码道三角波骨架增加测量结果的稳定性，最后利用径向基神经网络进行非线性补偿，减少绝对定位误差。实验结果表明，提出的位移测量方法能够实现快速、精确地量子点光栅尺高精度测量。相比于现有位移测量方式，提出的位移测量方法具有更高的测量精度、测量稳定性和测量速度。

参考文献

[1] LI D, WANG B, TONG Z, et al. On-machine surface measurement and applications for ultra-precision machining: a state-of-the-art review[J]. The International Journal of Advanced Manufacturing Technology, 2019, 104: 831-847.

[2] LIU C H, JYWE W Y, JENG Y R, et al. Design and control of a long-traveling nano-positioning stage[J]. Precision Engineering, 2010, 34(3): 497-506.

[3] MI X, ZHANG S, QI X, et al. Ruling engine using adjustable diamond and interferometric control for high-quality gratings and large echelles[J]. Optics Express, 2019, 27(14): 19448-19462.
[4] SEKKAT S, KOUISS K, SAADI J, et al. Developing integrated performance measurement system using component based approach[J]. International Journal of Computers Communications & Control, 2013, 8(2): 294-303.
[5] LI B, CAI H, MAO X, et al. Estimation of CNC machine-tool dynamic parameters based on random cutting excitation through operational modal analysis[J]. International Journal of Machine Tools and Manufacture, 2013, 71: 26-40.
[6] HEUER V, FARON D R, BOLTON D, et al. Distortion control of transmission components by optimized high pressure gas quenching[J]. Journal of Materials Engineering and Performance, 2013, 22: 1833-1838.
[7] LIN S T. A laser interferometer for measuring straightness[J]. Optics & Laser Technology, 2001, 33(3): 195-199.
[8] YANG F, ZHANG M, YE W, et al. Three-degrees-of-freedom laser interferometer based on differential wavefront sensing with wide angular measurement range[J]. Applied Optics, 2019, 58(3): 723-728.
[9] WANG H, LI M, CHEN X, et al. Novel linear optical encoder with absolute imaging position[C].2014 IEEE International Conference on Consumer Electronics-China, IEEE, 2014: 1-2.
[10] DZIWIŃSKI T. A novel approach of an absolute encoder coding pattern[J]. IEEE Sensors Journal, 2014, 15(1): 397-401.
[11] VOIGT D, ELLIS J D, VERLAAN A L, et al. Toward interferometry for dimensional drift measurements with nanometer uncertainty[J]. Measurement Science and Technology, 2011, 22(9): 094029.
[12] LACOT E, JACQUIN O, ROUSSELY G, et al. Comparative study of autodyne and heterodyne laser interferometry for imaging[J]. Journal of the Optical Society of America A, 2010, 27(11): 2450-2458.
[13] PENG Donglin, FU Min, CHEN Xihou, et al. Classification study on typical displacement sensors and analysis on the characteristics of time grating sensors[J]. Journal of Mechanical Engineering, 2018, 54(10): 36-42.
彭东林, 付敏, 陈锡侯, 等. 典型位移传感器分类研究与时栅传感器特点分析[J]. 机械工程学报, 2018, 54(10): 36-42.
[14] WANG H, WANG J, CHEN B, et al. Absolute optical imaging position encoder[J]. Measurement, 2015, 67: 42-50.
[15] SHI C, SHI G, SHI G, et al. Simulation and analysis of mechanical behavior of groove-shaped over-squeezing during mechanical ruling[J]. International Journal of Precision Engineering and Manufacturing, 2019, 20: 1107-1118.
[16] JEON T, KIM D H, PARK S G. Holographic fabrication of 3D nanostructures[J]. Advanced Materials Interfaces, 2018, 5(18): 1800330.
[17] TU M, XIA B, KRAVCHENKO D E, et al. Direct X-ray and electron-beam lithography of halogenated zeolitic imidazolate frameworks[J]. Nature Materials, 2021, 20(1): 93-99.
[18] WU L, HILBERS M F, LUGIER O, et al. Fluorescent labeling to investigate nanopatterning processes in extreme ultraviolet lithography[J]. ACS Applied Materials & Interfaces, 2021, 13(43): 51790-51798.
[19] SHAO J Y, CHEN X L, LI X M, et al. Nanoimprint lithography for the manufacturing of flexible electronics[J]. Science China Technological Sciences, 2019, 62: 175-198.
[20] WU H, JIAO Y, ZHANG C, et al. Large area metal micro-/nano-groove arrays with both structural color and anisotropic wetting fabricated by one-step focused laser interference lithography[J]. Nanoscale, 2019, 11(11): 4803-4810.
[21] ZHENG Liming. The accuracy detection equipment and the accuracy correction algorithm of absolute linear encoder product[J]. Development & Innovation of Machinery & Electrical Products, 2015, 28(4): 92-96.
郑黎明. 绝对式光栅尺产品的精度检测设备与精度修正方法[J]. 机电产品开发与创新, 2015, 28(4): 92-96.
[22] BAN J, CHEN G, WANG L, et al. A calibration method for rotary optical encoder temperature error in a rotational inertial navigation system[J]. Measurement Science and Technology, 2022, 33(6): 065203.
[23] LOPEZ J, ARTES M, ALEJANDRE I. Analysis under vibrations of optical linear encoders based on different scanning methods using an improved experimental approach[J]. Experimental Techniques, 2012, 36(6): 35-47.
[24] ZHAO L, CHENG K, CHEN S, et al. An approach to investigate moiré patterns of a reflective linear encoder with application to accuracy improvement of a machine tool[J]. Proceedings of the Institution of Mechanical Engineers, Part B: Journal of Engineering Manufacture, 2019, 233(3): 927-936.
[25] ZHANG D, LIN L, ZHENG Q. Error analysis and modeling for an absolute capacitive displacement measuring system with high accuracy and long range[J]. Sensors, 2019, 19(24): 5339.
[26] LOPEZ J, ARTES M. A new methodology for vibration error compensation of optical encoders[J]. Sensors, 2012, 12(4): 4918-4933.
[27] LI Yanfeng, YANG Zhijun, SUN Han, et al. Measurement system of macro-micro composite grating ruler based on virtual instrument[J]. Acta Photonica Sinica, 2018, 47(10):1012002.
李彦锋, 杨志军, 孙晗, 等. 基于虚拟仪器的宏微复合光栅尺测量系统[J]. 光子学报, 2018, 47(10):1012002.
[28] CAI N, XIAO P, YE Q, et al. Improving the measurement accuracy of an absolute imaging position encoder via a new

edge detection method[J]. IET Science, Measurement & Technology, 2017, 11(4): 406-413.
[29] LI W, CAI N, NING Z, et al. Error compensation for optical encoder via local-sinusoidal-assisted empirical mode decomposition with an optimization scheme[J]. IEEE Transactions on Industrial Electronics, 2021, 69(9): 9596-9604.
[30] BARAKAUSKAS A, BARAUSKAS R, KASPARAITIS A, et al. Error modelling of optical encoders based on Moiré effect[J]. Journal of Vibroengineering, 2017, 19(1): 38-48.
[31] WANG H, OU W, WU Z, et al. Quantum dot encoder via near-field direct writing[J]. IEEE Sensors Journal, 2022, 22(21): 20293-20302.

High-precision Measurement for a Quantum Dot Encoder Based on Triangular-wave Skeleton Extraction of Coding Patterns

WU Zhiliang[1], CAI Nian[1], OU Weicheng[2], CHEN Xiaona[1], WANG Han[2]
(1 *School of Information Engineering, Guangdong University of Technology, Guangzhou* 510006, *China*)
(2 *School of Electromechanical Engineering, Guangdong University of Technology, Guangzhou* 510006, *China*)

Abstract: The laser interferometer and the optical encoder are commonly used for high-precision displacement measurement, which is significant for equipment manufacturing. The former can realize sub-micron measurement by counting and subdividing interference fringes. However, it has the disadvantages of strict requirements for the measurement environment and difficult integration directly into the equipment, which greatly limit its applications in industrial measurement and control. Compared with the laser interferometer, the encoder has been widely integrated with the CNC machine as a core measurement component due to its advantages of low cost, small size, and simple optical structure. Grating lithography has been successfully employed to fabricate the gratings of optical encoders. However, some inherent problems exist in this fabricating process, such as low production, long production cycle, and harsh production conditions. Furthermore, the optical encoder manufactured by the grating lithography requires a combination of a light source and a reading head. When the encoder has worked for a long period of time, the light source will dissipate a large amount of heat, resulting in a drastic change in the internal temperature of the encoder. The drastic temperature change will cause the thermal deformation error of the encoder substrate to influence its measurement precision. Due to the advantages of high efficiency, low cost, and simple process requirements, we have introduced additive manufacturing with perovskite quantum dots to fabricate a novel linear encoder named quantum dot encoder, which prints the perovskite quantum dot coding patterns on the substrate via additive manufacturing. Then, machine vision is applied to process the continuous, regular and winding quantum dot code pattern in real time to achieve displacement measurement. As a novel linear encoder, its measurement precision is significant for its wide applications. In order to further improve the measurement precision of the quantum dot encoder, a displacement measurement method based on triangular wave skeleton extraction of coding patterns is proposed in this paper. First, considering the winding and continuous shapes of coding patterns of the quantum dot encoder, the boundary tracking method with variable steps is proposed to detect the edges of coding patterns in real time. The detection path of this method is always kept around the edge of the coding patterns, so only a few pixels need to be traversed to detect the edges. Then, triangular wave fitting is carried out on the middle lines of coding patterns to obtain the triangular wave skeletons of coding patterns, so as to improve the measurement stability and the subdivision linearity of displacement. Finally, because of the advantages of simple structure, fast convergence, easy deployment, and good approximationperformance for nonlinear functions, a Radial Basis Function (RBF) neural network is used to compensate for the nonlinear errors emerging in the quantum dot encoder. A laser interferometer is used as a baseline for linear displacement measurement. We compared the three waveforms to fit the measured signal, which are triangle wave, sine wave and square wave. The experimental results show that the triangle wave can well fit the measured signal with a high amplitude and a low error rate. To validate the RBF neural network on the measurement error compensation of the quantum dot encoder, a BP network, an LSTM network and an RBF neural network are individually used to compensate for the measured displacement data while other experimental conditions remain unchanged. The experimental results show that the RBF neural network is

superior to the other two neural networks in error compensation performance. To analyze the effect of three different steps in the proposed displacement measurement method, an ablation experiment is conducted. The experimental results show that the boundary tracking step with variable steps for coding pattern detection greatly accelerates the speed of boundary tracking. Compared with our previous work, the operation efficiency has increased by 108.86%. The coding pattern skeleton extraction method based on triangle wave fitting reduces the impact of environmental noise on the measurement precision, resulting in a reduction of the repetitive displacement error from ±8.695 μm to ±0.870 μm. The error compensation method based on the RBF neural network effectively compensates the nonlinear error of the quantum dot encoder, and improves the RMSE, maximum error, variance and confidence interval. Comparison experimental results indicate that the proposed method is more robust and achieves better measurement accuracy than the existing methods.

Key words: Machine vision; Quantum dot encoder; Measurement; Boundary tracking; Skeleton extraction
OCIS Codes: 120.3940; 150.0155; 130.3990; 130.6010

Foundation item: National Natural Science Foundation of China (No. 62171142), National Natural Science Foundation of Guangdong Province (No. 2021A1515011908), Research Fund for Colleges and Universities in Huizhou (No. 2019HZKY003)